HiSST: 3rd International Conference on
High-Speed Vehicle Science Technology
14 -19 April 2024, Busan, Korea

High Performance Wall Heat Flux Surrogate Models for vehicles/capsules design activities and Space Debris ground risk estimation – Review of ONERA recent developments

Y. Prevereaud[1]

Abstract

An accurate determination of the wall heat flux in hypersonic regime is crucial for the design of any space vehicle and mission as well as for space debris survivability analysis. During vehicle pre-design and design phases, as well as space debris atmospheric entry prediction, analytical models are used to quickly estimate wall heat flux levels. Existing models in the open literature are either applicable to specific flow conditions and/or only applicable to a limited number of shapes, and/or depend on local parameters not accessible by engineering approaches. Moreover, even though the models are used within their valid range, a high level of uncertainty is generally associated with such obtained solutions. Thus, ONERA has been developing new surrogate models in hypersonic regime from rarefied to continuum flow conditions to improve its capability to describe trajectory ATD processes with a significant increase of accuracy. The aim of the present paper is a focus on the very last analytical formulations, developed to characterize stagnation point heat flux and 3D wall heat flux distribution levels in various flow regimes for any kind of flying shape.

Keywords: *surrogate model, heat flux, aerothermodynamic, atmospheric entry, TPS design*

1. Introduction

The correct prediction of both wall heat flux and wall temperature in the hypersonic regime is an essential prerequisite for the design of any space vehicle and mission as well as for the accurate estimation of the ground risk consecutive to space debris atmospheric entries. Heat flux must be assessed as accurately as possible to avoid any oversizing of TPS or to under/over-estimate the ground risk generated by survival space debris impacts. Although the high-fidelity physical models are relatively accurate, they are unable to explore, in a short time (few minutes), a large number of vehicle designs, multiple trajectories and different Thermal Protection System (TPS) in the predesign phase, especially during Concurrent Design Engineering activities. Moreover, they cannot be used to determine a whole trajectory of several debris fragments and even less to assess multiple trajectories needed for Monte Carlo approaches. Only a strategy based on relevant and reliable reduced models appears acceptable in terms of computing time and simulation capability. Therefore, space actors have developed specific engineering tools and Multidisciplinary Design Analysis and Optimization (MDAO) approaches, as ARES (Atmospheric Re-Entry Software) at ONERA, using surrogate models to calculate wall heat flux and temperature levels. However, the current heat flux models have been developed for both limited configurations (flight points or shapes) and physical phenomena.

Most of the models in open literature have been derived assuming a thermochemical equilibrium flow, with laminar boundary layer, and catalytic wall. Existing formulations assuming particular physical phenomena (such as turbulent boundary layer or finite catalytic wall) are either only applicable to a limited number of shapes, or depend on local parameters that are so far unreachable *a priori* by engineering codes. Moreover, even though a model is used within its valid range, a high level of uncertainty remains associated with the obtained solution.

[1] *ONERA/DMPE, Université de Toulouse, F-31055 Toulouse – France, ysolde.prevereaud@onera.fr*

For instance, in continuum hypersonic regime, Detra [1], Scott [2], Sutton-Graves [3], Vérant-Sagnier [4] models, compute the stagnation point heat flux for both thermochemical equilibrium or chemical non-equilibrium gases, assuming full catalytic walls. Even though Fay-Riddell [5] proposed a formulation to compute stagnation point heat flux for a frozen gas with non-catalytic wall, such a model requires many local quantities that are not easily accessible for engineering codes. Similarly, a number of models can be found in the literature for determining the distribution of wall heat flux of objects of different shapes. Those models generally consider the ratio between the local heat flux and the stagnation point heat flux, and not directly the local heat flux. Lees [6], Kemp [7] or Murzinov [8] models were developed for specific geometric shapes. However, other models in the literature claim to be more generalist, such as Vérant-Lefrançois model [9] or the model used in the Spacecraft-Oriented code SCARAB [21]. The comparison between the results obtained with literature models and CFD simulations for different types of shapes (Fig. 1) reveals that most of the models give satisfying results for convex blunted objects (Fig. 2). However, all these models cannot predict wall heating in a number of situations: concave walls, flat walls (Fig. 3), trailing edge boundary layer thinning, shock-shock interactions or shock-boundary layer interactions.

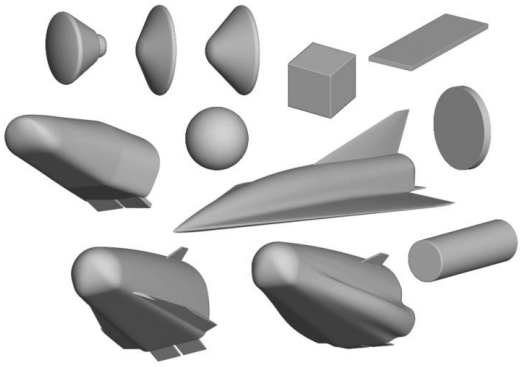

Fig. 1. Objects shapes of the numerical database.

In hypersonic rarefied regime, bridging functions $f_b(.)$ are used according to the following relationship:

$$C_{x,rar} = C_{x,cont} + \left(C_{x,fm} - C_{x,cont}\right) f_b(Kn) \tag{1}$$

where Kn is the Knudsen number that measures the degree of rarefaction of the gas, and the bridging function verifies $f_b(Kn_{cont}) = 0$, $f_b\left(Kn_{fm}\right) = 1$ where Kn_{cont} and Kn_{fm} are the Knudsen numbers indicating the limits of the continuum and free molecular regime respectively. Moreover, $C_{x,rar}$ is any global (aerodynamic forces and moments coefficients as C_D, C_L) or local coefficient (pressure C_p, friction C_f, heat flux C_h coefficients) in the rarefied regime (i.e. such as $Kn_{cont} \leq Kn \leq Kn_{fm}$) and $C_{x,cont}$, $C_{x,fm}$ respectively denote the value in the continuum and free molecular regimes.

Since the first bridging function proposed by Martino [10], several formulations were derived [11–15]. Their application to flight data [16] have for instance proved the relevance of such method for the reconstruction of the C_A/C_N ratio measured during the Viking I entry into the Mars atmosphere. Nevertheless, when the bridging function is not parametrized for a specific object, its generalization capacities suffer from the relative aspect of the rarefaction parameter ($Kn = \lambda_\infty/L_{ref}$) which is highly dependent on the choice of the reference length. Moreover, the non-absolute value of the continuum and free molecular limits in terms of Knudsen number is another important limitation. Eventually, as evident from equation (1), the error due to the distribution formulations in the limit regimes fatally propagates through the rarefied transitional regime. Thus, with the aim of improving the preciseness of the panel methods in the rarefied regime, Falchi carried out dedicated efforts in the frame of his Ph.D. [17]. However, Falchi's work mostly focuses on sharp geometries (as cube and cylinder) characteristic of debris shapes while we are more concerned with aerodynamic shapes.

The development of more complete and more generalist wall heat flux models (i.e. not attached to a specific shape as far as possible), accounting for complex physical phenomena (non-catalytic wall, turbulent boundary layer, etc.), is then mandatory.

For several years, ONERA has been conducting research in this direction and developed new surrogate models in hypersonic regime, from rarefied to continuum flow conditions. Different methods have been used to reach this goal: classical formulations as well as neural network-based models. The objective of the paper is to present the most recent developments in the modeling of the stagnation point heat flux and the three-dimension wall heat flux distribution.

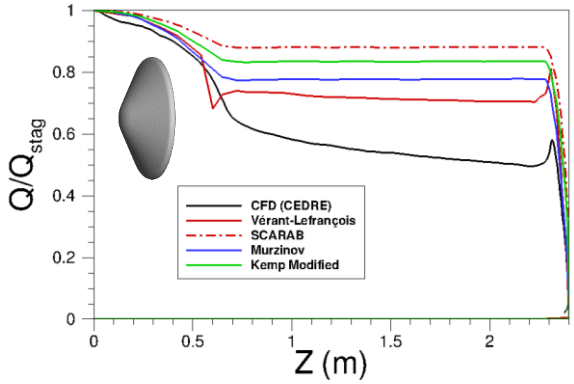

60° Sphere-cone - Mach 25, Z = 75 km, $\alpha = 0°$

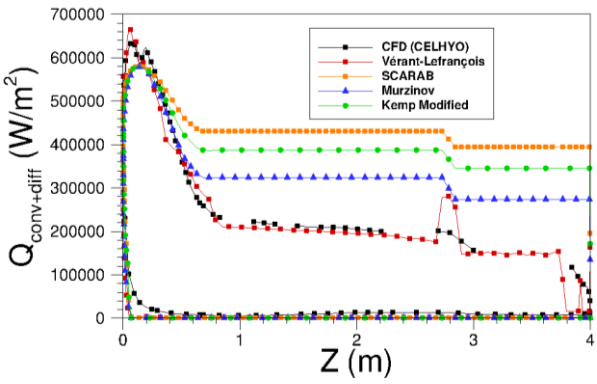

PRE-X vehicle - Mach 25, Z = 74 km, $\alpha = 40°$

Fig. 2. Comparison of wall heat flux distribution obtained with analytical models and CFD simulations for convex objects.

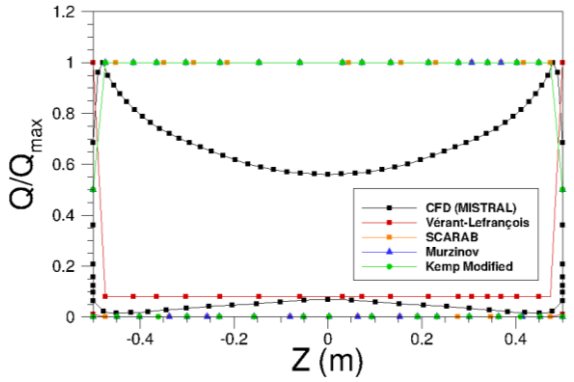

Cube – Mach 20, Z = 70 km, $\boldsymbol{\alpha = 0°}$

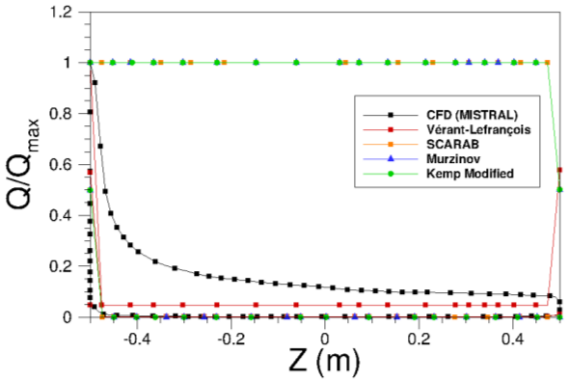

Cube – Mach 20, Z = 70 km, $\boldsymbol{\alpha = 45°}$

Fig. 3. Comparison of wall heat flux distribution obtained with analytical models and CFD simulations for a cube with and without angle of attack $\boldsymbol{\alpha}$.

2. Strategy for model development

As explained above, most of models in the open literature have been developed for specific flow assumptions; furthermore, the use of these models in their valid parameters range does not guarantee the accuracy of the solution. In consequence, the strategy adopted at ONERA has been 1) to increase the accuracy of the existing models; 2) to develop more complete and/or more generalist models.

The development of surrogate models follows four main steps:

1) Identify the most relevant parameters having an influence on the quantity to model. A preliminary analysis of the existing models as well as CFD and/or experimental results is therefore necessary at first. In addition, to ensure the generalization of the model, input and output variables must be expressed through appropriate non-dimensional numbers.

2) Determine the range of variation of the input parameters to ensure that the future model can be used on its whole applications range.

3) Generate a database for the model development/training (~ 80% of the database) and its validation (~ 20% of the database). Such database must then cover the whole range of the input variables.

   The database is built using CFD Navier-Stokes structured or unstructured codes (CELHYO and CEDRE/CHARME from ONERA, LORE from ESA, MISTRAL from RTech) in continuum regime and DSMC code (SPARTA from Sandia Lab.) in rarefied regime.

   The fact that the numerical database used consists of mixing results from different CFD codes with different models, numerical parameters, can be seen in different ways. On the one hand, there is an uncertainty associated with the numerical results obtained. This can be determined/estimated thanks to the existence of several solutions on the same case (numerical dispersion). On the other hand, the model developed from this database should be expected more robust, as it will integrate a wide range of solutions from different horizons.

4) Develop and validate the model.

For this fourth step, different approaches can be used like simplification of Euler equations, data fitting with mathematical functions or various machine learning (ML) methods like regression (linear Bayesian, Kriging), genetic programming, Neural Network (NN) and Deep learning. The development of the database and the type of approach used to develop the model are closely linked. For example, NNs are suitable when the amount of data is large, while Kriging methods can be used when lesser amount of data are available. Moreover, the way the database is built (third step in the list above) is also very important and depends on the type of modeling that will be applied. Indeed, for an optimal use some methods require a specific design of experiments (DOE), i.e. the distribution of the sample points within the range of variation of the input parameters. For example, for Kriging, this range must be fully explored avoiding variation of one input parameter at a time (OAT); a Latin Hypercube Sampling (LHS) DOE is mandatory. These two kinds of DOE are illustrated in Fig. 4 in two dimensions, i.e. corresponding to two input parameters. However, one can easily conceive that, to understand and determine which parameters have an influence on the quantity to model (first step in the list above), it is necessary to vary the values of one parameter at a time. It is therefore necessary to build a first database allowing to identify the main driving parameters of the physical phenomena. Then, once the range of variation of these parameters is fixed (second step in the list above), a second database is created for the model development.

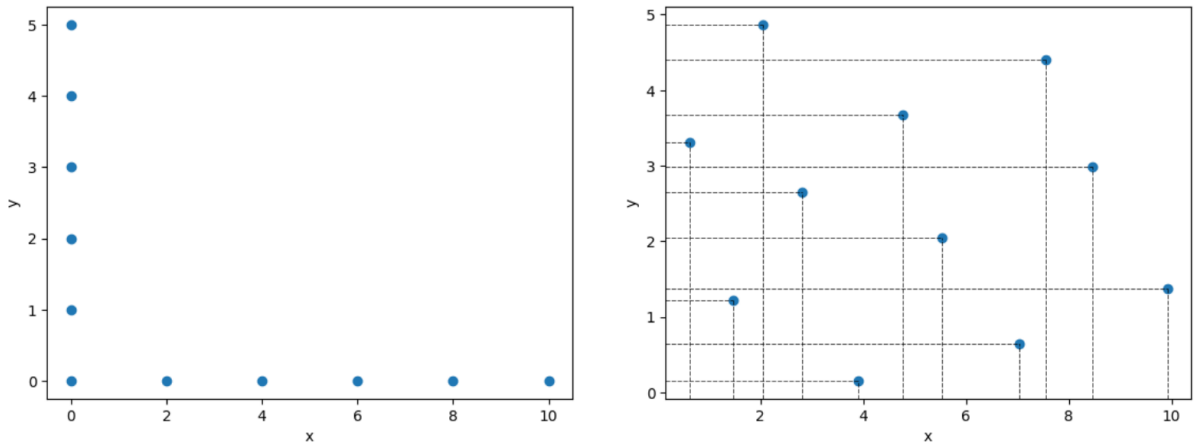

Fig. 4. Example of two kind of DOE: One At a Time (OAT) on the left and Latin Hypercube Sampling (LHS) on the right [18].

3. Heat flux stagnation point models

3.1. Heat flux stagnation point models in hypersonic continuum regime

In hypersonic continuum regime, four of the existing models (Vérant-Sagnier, Vérant-Lepage, Sutton-Graves, Fay-Riddell) used to predict the stagnation point convective-diffusive heat flux, assuming laminar boundary layer and catalytic wall, were compared to 42 CFD results to evaluate the relative error.

Table 1. Min, Max, Mean relative error (%) between results from CFD and models from literature

Relative Error (%)	Sutton-Graves	Vérant-Sagnier	Fay-Riddell	Vérant-Lepage
Min	8.14	0.48	0.02	0.93
Max	22.73	14.24	14.37	35.95
Mean	13.27	4.85	5.53	14.40

The models are considered satisfactory if the mean relative error is less than 5% and the max relative error is inferior or equal to 10%. As illustrated in Table 1, the models proposed in the literature are not able to predict the stagnation wall heat flux with sufficient accuracy.

So, the parameters (see Table 2) of three of these empirical equations (Vérant-Sagnier, Vérant-Lepage, Sutton-Graves) were optimized using various machine-learning techniques, such as least square minimization algorithm and Kriging method. The Fay-Riddell model has not been considered since it requires information at the edges of the boundary layer not directly accessible by engineering atmospheric entry codes. Vérant-Lepage model, with eight parameters to optimize without physical meaning, is the most adaptable/flexible model. Conversely, for the Sutton-Graves model, only ywo parameters having physical meaning can be optimized. For this optimization process, a database composed of 60 CFD simulations is established considering the following range of the input parameters: $V_\infty[m/s] \in [2000, 8000]$, $Rn\,[m] \in [0.1, 10]$, $T_w\,[K] \in [300, 2000]$, $H[km] \in [40, f(Kn)]$; the maximal altitude depending of other parameters to ensure continuous flow regime ($Kn < 10^{-3}$). The previous 42 CFD simulations are used for validation purpose. The results obtained with the optimized models are presented in Table 3. For the optimized Vérant-Lepage equation, the mean and the max relative error are 2.2% and 8.8% respectively. The Vérant-Sagnier and Sutton-Graves optimized model do not allow to obtain mean and max errors inferior to the imposed thresholds.

Table 2. Optimised empirical models

Empirical equations	Parameters
Vérant-Sagnier $$q_{stag} = a\sqrt{\frac{P_{stag}}{Rn}}\left(\frac{H_\infty - H_w}{287 \times 273.15}\right)^b$$	a, b
Vérant-Lepage $$q_{stag} = a + \left[b\rho_\infty^c \times Rn^d \times (V_\infty - f)^e\right]\left[1 - g\frac{(Cp(T_w)T_w - Cp(T_{ref})T_{ref})}{0.5V_\infty^2 - Cp(T_{ref})T_{ref}}\right]^h$$	a, b, c, d, e, f, g, h
Sutton-Graves $$q_{stag} = k_b\left(\frac{\rho_\infty}{Rn}\right)^{0.5} V_\infty^b$$	k_b, b

Table 3. Min, Max, Mean relative error (%) between results from CFD and optimised models

Relative Error (%)	Sutton-Graves	Vérant-Sagnier	Vérant-Lepage
Min	2.6	0.3	0.1
Max	45.6	13.4	8.8
Mean	13.1	4.1	2.2

To complement above models, an empirical model providing mass fraction of atomic species at the non-catalytic wall was developed by ONERA [19] in 2018. This model allows to compute the wall

enthalpy used in the correlations proposed in literature (Sutton-Graves, Fay-Riddell, Vérant-Sagnier and Vérant-Lepage) to determine the stagnation point heat flux for non-catalytic wall. In addition, for finite catalytic wall, a bridging function has been developed. These models were built on a CFD database including 190 computational results, represented by the black square in Fig. 5, and calibrated for various upstream flow conditions (altitude from 70 to 20 km, velocity from 8 to 2 km/s) leading to different thermochemical flow conditions in the shock layer (perfect gas, frozen gas, thermochemical equilibrium and chemical nonequilibrium gas), effects of the nose radius (from 0.01 m to 10 m), wall temperature (from 300 K to 2000 K), and recombination coefficient (from 0 non catalytic to 1 fully catalytic). However, as illustrated in Fig. 5, a part of the variation domain of input parameters was still unexplored. So, new CFD simulations have been performed to complete the database and to extend the min and max values of the input data: $V_\infty[m/s] \in [2000, 8000]$, $Rn\,[m] \in [0.01, 10]$, $T_w\,[K] \in [300, 3000]$, $H[km] \in [20, 80]$. Then the model for the mass fraction of atomic species has been revised based on this extended database. As illustrated in Fig. 6, the stagnation point heat flux, calculated with Sutton-Graves model (for example) using the mass fraction model developed, is successfully compared to the CFD results.

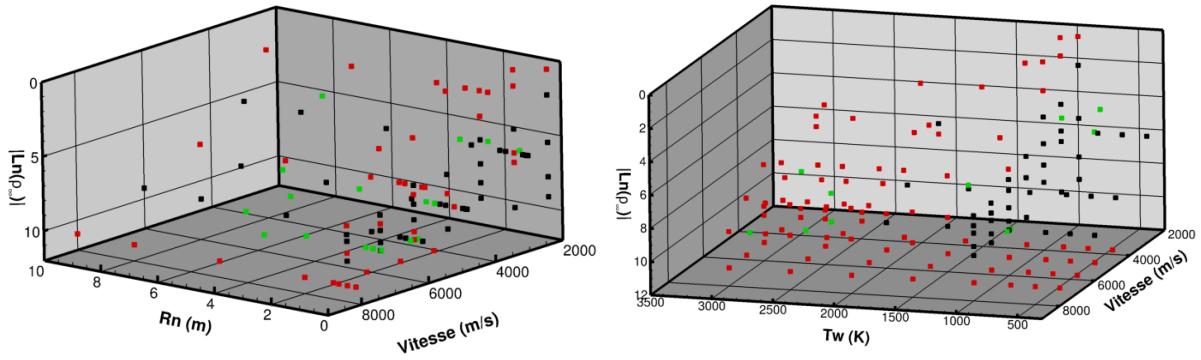

Fig. 5. Visualisation of the CFD database (in black: cases included in the preliminary database; in red: new cases added in the database; in green: validation cases).

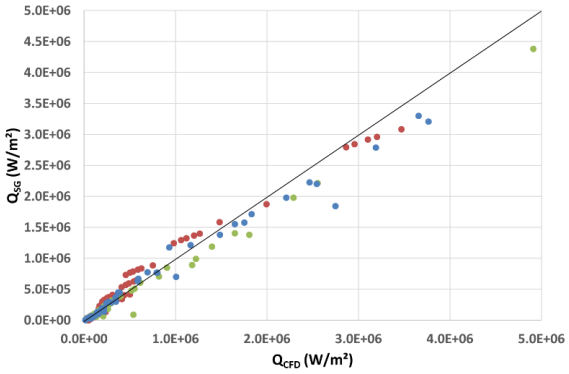

Fig. 6. Comparison between CFD (abscissa) and new analytical model (ordinate) for stagnation point heat flux assuming non-catalytic wall.

3.2. Heat flux stagnation point models in hypersonic rarefied regime

In hypersonic rarefied regime, the well-known bridging functions between continuum and free molecular regimes are commonly used. However, the accuracy of the results depends on the accuracy of the models used in both continuum and free molecular regimes. To avoid this strong dependence, a new model using only local freestream and geometrical quantities was developed based on Kriging methods

In hypersonic rarefied conditions, the most relevant nondimensional numbers are the Knudsen and Mach numbers. In addition, the literature and the engineering models exhibit that under the fully diffusion wall assumption, the stagnation heat flux coefficient can be computed from a few contextual quantities (e.g. ρ_∞, T_∞, $R_{S,air}$, V_∞, Rn). Since the Knudsen and the Mach numbers encompass all the environmental values and according to the machine learning principle which recommends to avoid redundant information, these two numbers appear as the most natural candidates. By noticing that the

reference length L_{ref} used in the Knudsen number calculation depends on the context, the following choice $L_{\text{ref}} = 2Rn$ (with Rn the stagnation point curvature) allows for the most relevant geometric quantity to be included into the design variables. The surrogate model for the stagnation point heat flux coefficient C_h was then chosen as follows:

$$C_{h,stag} = f(Kn, M_\infty) = f\left(\frac{\lambda_{N_2,\infty}^{VHS}}{2Rn}, \frac{V_\infty}{\sqrt{\gamma R_{S,air} T_\infty}}\right)$$

To develop and validate the model [20], CFD (CEDRE and CASL ONERA codes) and DSMC (SPARTA code) databases were built for the following exploration domain: nose radius Rn ϵ [0.1; 50] m, altitude z ϵ [85; 200] km and upstream velocity ϵ [6; 10] km/s. These variables impose the limits of the physical domain in terms of Mach/molecular speed ratio according to the Knudsen number range Kn ϵ [10^{-3}; 100]. 25 2D-axysymmetric DSMC and CFD computations were performed to train the model. For the validation, Singh and Schwartzentruber work [23] provided 29 points inside the plan of experiments for the validation of the $C_{h,stag}$ prediction model. In addition, 23 validation points for the $C_{h,stag}$ prediction model were extracted from the DSMC 3D database performed on 3D geometries (Apollo, OREX and IXV) and used for the training of the neural network models (see Section 4.2).

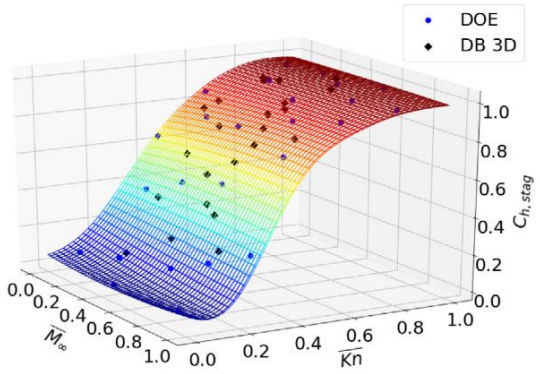

Fig. 7. Comparison of $C_{h,stag}$ obtained with kriging technic (Gaussian kernel) and DSMC [20].

Different kind of Kernel (Gaussian, exponential, matern52) were tested for the kriging interpolation method. A global S shape is observed as expected with a small dependence on the Mach number. The Gaussian kernel (Fig. 7) provides the smoothest and the most relevant response while the exponential correlation function is, as expected, noisier. The root mean squared (RMSE) and the mean relative errors (MRE) obtained with the different models are summarized in Table 4.

Table 4. Errors in the $C_{h,stag}$ prediction obtained with various reduced models. The corresponding validation database is indicated between brackets.

Surrogate model	RMSE (%) [Singh]	MRE (%) [Singh]	RMSE (%) [DB 3D]	MRE (%) [DB 3D]
Gaussian kriging	0.056	4.349	0.0541	6.046
Exponential kriging	0.064	5.534	0.0529	5.789
Matern52 kriging	0.0576	4.499	0.0531	5.803

Whatever the model used, the MRE is around 5% which is quite remarkable according to the wide variation range of $C_{h,stag}$. Comparatively, a mean relative error comprised between 12.2% and 13.1% was obtained with the literature models implemented in the ONERA ARES code.

4. Wall heat flux distributions

4.1. Heat flux distribution model in hypersonic continuum regime

For the development of a new heat flux distribution model in hypersonic continuum regime, an extensive numerical database composed of 2D-axisymmetric and 3D Navier-Stokes simulations around a wide

variety of shapes (Fig. 1), objects attitude (angle of attack α, side slip angle β) and flight points (altitude, velocity) have been used. The object size in the database is between 0.05 m and 65 m. According to the considered object, α and β varies from 0° to 90°. In terms of flight points, a wide range of altitude-Mach number has been considered along characteristic spacecraft and space debris characteristic trajectories: $30\ km\ \leq Z \leq 90\ km$, $2 \leq M_{\infty} \leq 35$.

The analysis of the models described in the literature as well as the analysis of the CFD database made it possible to highlight driver parameters having a strong influence on the distribution of dimensioned heat flux: the pressure ratio $\frac{P(x,y,z)}{P_{stag}}$, the Mach number M_{∞}, at least one geometric quantity and the object attitude (α, β).

The model was developed following the strategy described below:

- A first parametrization of the model was done with spherical shape;
- Followed by a wide variety of convex shapes were considered;
- finally, specific developments were proposed to deal with flat surfaces.

The ratio between the local heat flux and the stagnation point heat flux calculated using the newly developed model (denoted "New model" in the figures) has been compared with the CFD results as well as with results obtained with the Vérant-Lefrançois model (denoted "Old model" in the figures) for different geometric shapes: capsules, vehicles, cubes/flat plates and cylinders.

In the case of the sphere-cone of 60° half-cone-angle in incidence of 15° (Fig. 8 and Fig. 9), the heat flux calculated using the new surrogate model makes it possible to obtain solutions very close to the numerical values both on the spherical part and the conical part, unlike the heat flux calculated with the Vérant-Lefrançois model. On the other hand, the difference between the numerical and analytical values increases around the shoulders of the sphere-cone, inducing a significant error at this location. In the case of the 'Baseline'' shape (Fig. 10 and Fig. 11) of Hypmoces (escape vehicle of the SpaceLiner defined during a EU FP7 project), the heat flux calculated by the new surrogate model is in very good agreement with the heat flux obtained by numerical simulation whether on the convex part or the flat part of the vehicle.

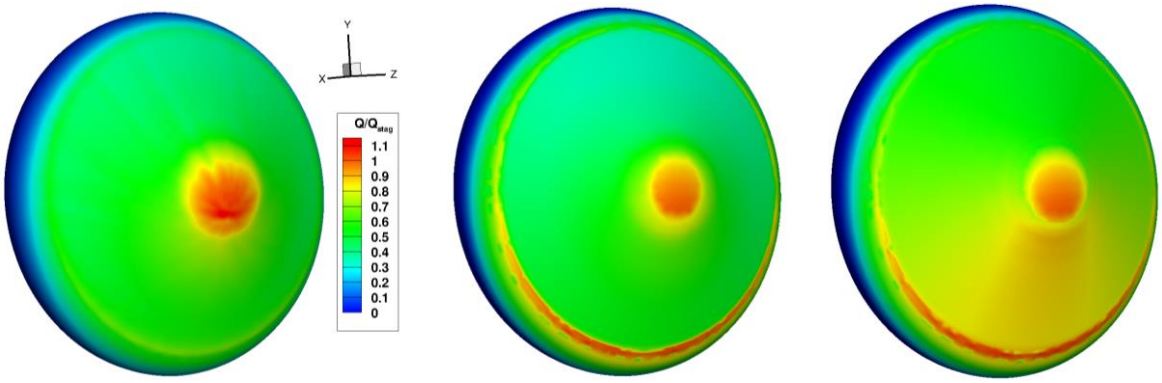

Fig. 8. Wall heat flux distribution for a 60° sphere-cone – Mach 22, $\boldsymbol{\alpha = 15°}$.

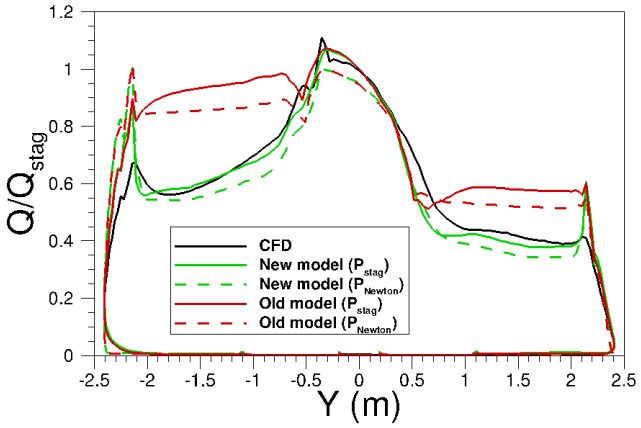

Fig. 9. Wall heat flux distribution along the center line of the 60° sphere-cone – Mach 22, $\boldsymbol{\alpha = 15°}$.

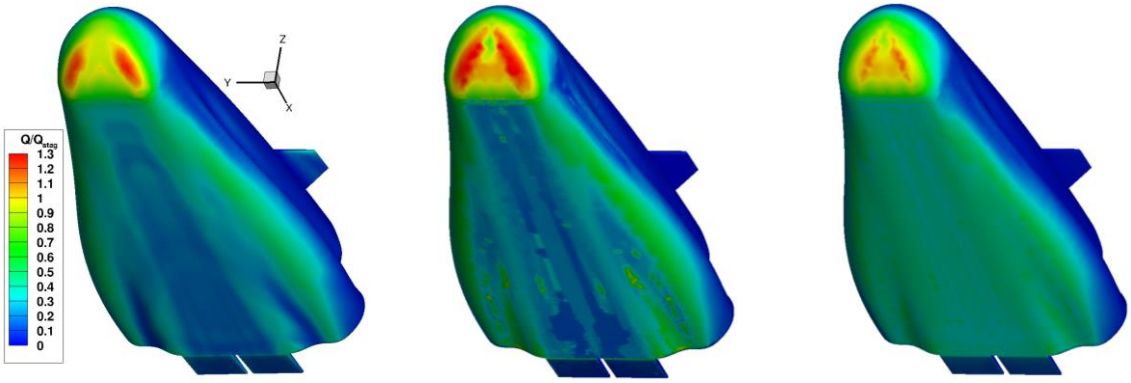

Fig. 10. Wall heat flux distribution at the wall of the Hypmoces vehicle – Mach 20, $\boldsymbol{\alpha = 35°}$, $\boldsymbol{\beta = 0°}$ in continuum regime.

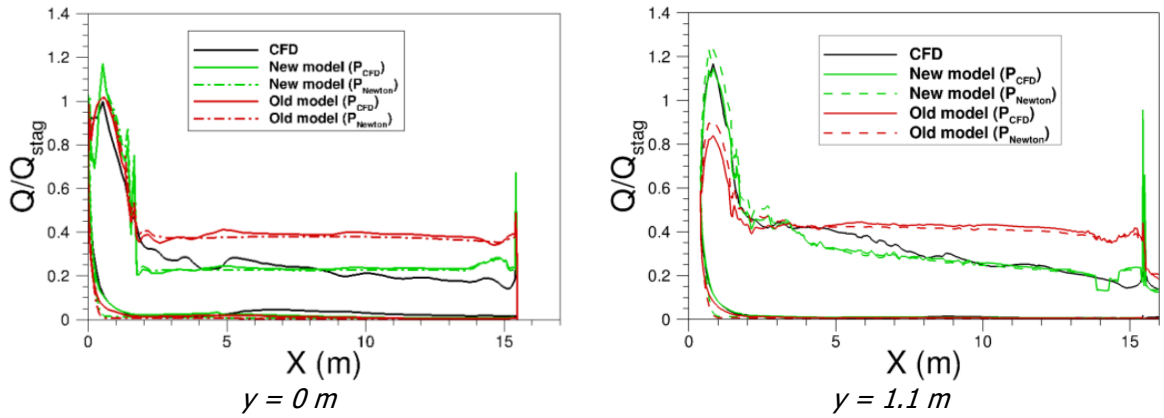

Fig. 11. Wall heat flux distribution along different cutting plan (y = 0 m and y = 1.1 m) of the Baseline shape of the Hypmoces vehicle – Mach 20, $\boldsymbol{\alpha = 35°}$, $\boldsymbol{\beta = 0°}$.

In general, this new model provides solutions in good agreement with the CFD solutions on a wide variety of objects shapes and flight conditions. A significant improvement of the results is then obtained with this new surrogate model compared to those from open literature.

4.2. Heat flux distribution model in hypersonic rarefied regime

The analysis of the simulations performed in the frame of previous studies [24-26] for various atmospheric entry vehicles (Apollo 6, Apollo AS-202, OREX and the IXV) as well as the analysis of the current models enabled identification and confirmation of the most relevant design variables that are to be accounted for in the new model. A model in the form of $C_h = f\left(C_{h,stag}, \alpha, d_{stag}, \frac{Rn}{Rn_{loc}}\right)$ was

retained. As opposed to the kriging model for $C_{h,stag}$ where the design variables (Kn, M_∞) are global, input parameters for C_h distribution are local. Consequently, each simulation provides as many sampling points as many of surface elements on the geometry. However, all models also depend on a stagnation quantity and since one simulation only provides one set of stagnation values, exploration of the plan of experiments is less extensive. A DOE was built with the objective of homogeneously exploring the vehicle design space. Hence, because varying thoroughly each geometric variable across its interval of variation ($\alpha \in [-90°; 90°]$, $\frac{Rn}{Rn_{loc}} \in [0; 10]$, $d_{stag} \in [0; 4]\,\mathrm{m}$) is hard with a fixed set of only 3 geometries (Apollo, OREX, IXV), the database was built with the following constraints: 1) Ensure that the sampling points cover a maximal area of the design space. 2) Minimize the number of simulations to do so. A 3D database was generated from a pseudo-random sampling of a vehicle, an altitude ($h \in$ [95; 150] km), a velocity ($V_\infty \in [6; 10]\,\mathrm{km/s}$) and an angle of attack ($\alpha \in [0°; 180°]$). A total of 27 simulations has been performed homogeneously exploring both the local variables spaces and the range of altitude.

For the surface coefficients, the large amount of data to learn (around 300 000 sample points) make Artificial Neural Network (ANN) one of the most suited methods. The results obtained with the new ANN model developed are compared to the ones calculated by the DSMC and classical empirical models implemented in ARES code in Fig. 12 and Fig. 13 for OREX and SpaceLiner vehicles respectively. Extensive comparison can be found in [20]. For the OREX case, whose geometry has been included into the training database, heating coefficient contours indicate a 3 to 8% relative difference between the ANN and DSMC results in the nose region. As for the distribution tendency, the comparison with ARES shows a poorer behaviour along the spherical section but a better capture of the heat flux diminution along the conical portion of the vehicle. For the SpaceLiner (not included into the training database and being much bigger than the IXV - 65 m length compared to around 5 m length), the preliminary results were very poor as a consequence of using an absolute distance as a design parameter. It suggests that some kind of non-dimensional parameters might be more appropriate to deal with such geometries. In first approach, scaling the Spaceliner d_{stag} parameter according to the maximal value in the training database yields a much better result (illustrated in Fig. 13).

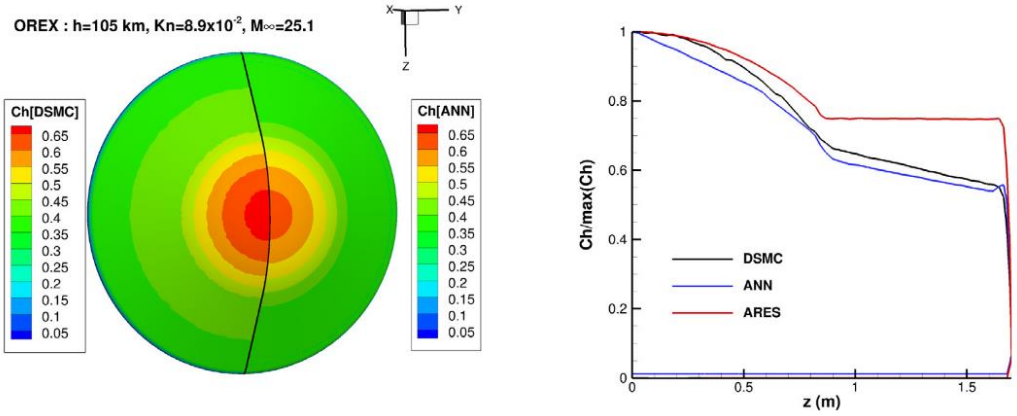

Fig. 12. Comparison of the C_h coefficient obtained with the neural network (ANN), with SPARTA (DSMC) and with ARES for OREX – Mach 25.

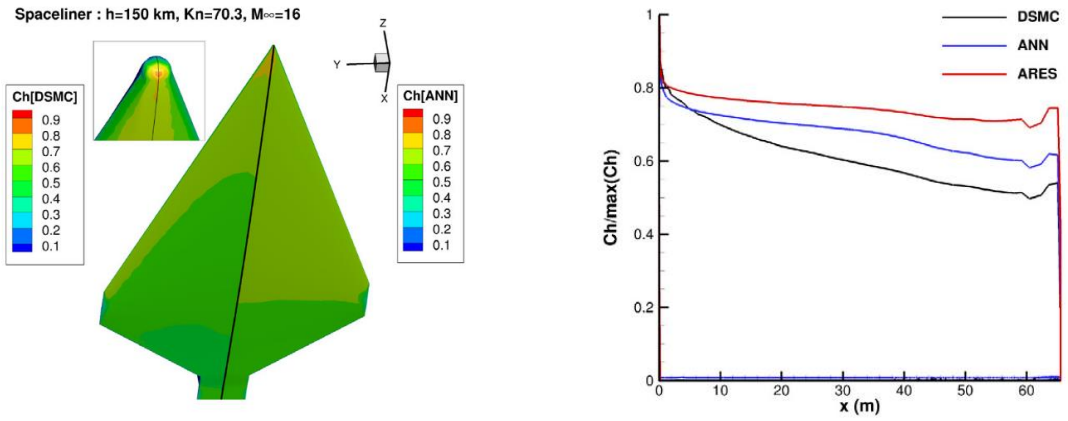

Fig. 13. Comparison of the C_h coefficient obtained with the neural network (ANN), with SPARTA (DSMC) and with ARES for the SpaceLiner – Mach 16.

The results obtained with ANN model showed that statistical learning methods are capable of performing similarly to classic methods and to outperform them in their limiting cases. When combined, the coupling of the kriging model for the stagnation point heat flux coefficient $C_{h,stag}$ and ANN model for the heat flux distribution [$C_h = f\left(C_{h,stag}, \alpha, d_{stag}, \frac{Rn}{Rn_{loc}}\right)$] address the main limitations of the existing methods based on bridging functions. Indeed, since the choice of the reference length for the calculation of the Knudsen number is fixed/imposed, the model can be easily generalized. In addition, they are capable of computing the wall heat flux under a non-catalytic wall assumption in rarefied regime, close to the continuum regime, which is not possible with the current formulations. The results showed that these models are ready to be used as such in a re-entry code like ARES.

5. Conclusion

New generalist models developed are now capable to express stagnation point heat flux for catalytic and finite catalytic walls assumptions as well as 3D wall heat flux distribution for any kind of shape in rarefied and continuum flow regimes. The performances of these new models is significantly better than the previous ones, allowing to reduce the error and margins taken in the pre-design methodology devoted to a space vehicle. These updated models were built and validated thanks to an extensive CFD and DSMC databases development. Each geometry of the database brings a large amount of learning points, identified as surface meshes or points. The construction of non-dimensional input and output variables is an important step in generalizing models applications. This principle is fully illustrated with the neural network model developed in the rarefied regime: indeed, the learning process of neural network (ANN) was done with three types of vehicle whose size did not exceed 5 m in length, while the validation was performed on the 65m-long SpaceLiner vehicle, off of the learning process.

References

1. Detra, R.W., Kemp, N.H., Riddell., F.R.: Addendum to Heat transfer to Satellite Vehicle Reentering the Atmosphere. Jet Prop. (1957). https://doi.org/10.2514/8.12510
2. Scott, C.D., Ried, R.C., Maraia, R.J., Li, C.P., Derry, S.M.: An AOTV Aeroheating and Thermal Protection Study. Prog. Astronautics Aeronautics (1985). https://doi.org/10.2514/6.1984-1710
3. Sutton, K., Graves Jr., R.A: A General Stagnation-Point Convective Heating Equation for Arbitrary Gas Mixtures. NASA TR R-376 (1971).
4. Sagnier, P., Vérant, J-L.: Flow Characterization in the ONERA F4 high enthalpy wind tunnel. AIAAJ (1998). https://doi.org/10.2514/2.425
5. Fay, J.A., Riddell, F.R.: Theory of Stagnation Point Heat Transfer in Dissociated Air. J. Aero. Sci. (1958). https://doi.org/10.2514/8.7517
6. Lees, L.: Laminar Heat Transfer Over Blunt-Nosed Bodies at Hypersonic Flight Speeds. J. Jet Prop. (1959). https://doi.org/10.2514/8.6977

7. Kemp, N., Rose, P., Detra, R.: Laminar Heat Transfer Around Blunt Bodies in Dissociated Air. ARS J. (1959). https://doi.org/10.2514/8.8128
8. Murzinov, N. Laminar Boundary Layer on a sphere in Hypersonic Flow of Equilibrium Dissociating Air. Fluid Dyn. (1966). https://doi.org/10.1007/BF01013841
9. Prévereaud, Y., Vérant, J-L., Balat-Pichelin, M., Moschetta, J.-M.: Numerical and experimental study of the thermal degradation process during the atmospheric re-entry of a TiAl6V4 tank. Acta Astronautica. (2016). https://doi.org/10.1016/j.actaastro.2016.02.009.
10. Martino, R.L.: Heat Transfer in Slip Flow, Tech. rep., Institute of Aerophysics, University of Toronto, UTIA Report 35. (1955).
11. Masson, D.J., Morris, D.N., Bloxsom, D.E.: Measurements of Sphere Drag from Hypersonic Continuum to Free-Molecular Flow. Tech. rep. U.S. Air Force. (1960).
12. Matting, F.W.: Approximate bridging relations in the transitional Regime between continuum and free-molecule flows. J. Spacecr. Rockets. (1971). https://doi.org/10.2514/3.30214
13. Blanchard, R.C.: Rarefied flow lift-to-drag measurements of the Shuttle Orbiter. ICAS-86-2.10.2. (1986).
14. Blanchard, R.C.: Rarefied-flow aerodynamics measurement experiment on the aeroassist flight experiment vehicle. J. Spacecr. Rockets. (1991). https://doi.org/10.2514/3.26256
15. Ivanov, M.S., Markelov, G.N., Gimelshein, S.F.: High-altitude capsule aerodynamics with real gas effects. J. Spacecr. Rockets. (1998). https://doi.org/10.2514/3.26992
16. Wilmoth, R.G., Blanchard, R.C., Moss, J.N.: Rarefied transitional bridging of blunt body aerodynamics. 21st International Symposium on Rarefied Gas Dynamics. (1998).
17. Falchi, A.: Atmospheric Re-Entry Analysis of Space Objects (Ph.D. thesis). University of Strathclyde. (2020).
18. Drouet, V.: Modélisation aérothermodynamique des écoulements hypersoniques d'arrière-corps de débris orbitaux (Ph.D. thesis). Université de Toulouse. (2019).
19. Prévereaud, Y., Vérant, J-L., Annaloro, J. : Noncatalytic and Finite Catalytic Heating Models for Atmospheric Re-entry Codes. 1st IOC Conf. (2019).
20. Schouler, M., Prevereaud, Y., Mieussens, L.: Machine Learning based reduced models for the aerothermodynamic and aerodynamic wall quantities in hypersonic rarefied conditions. Acta Astronautica. (2023). https://doi.org/10.1016/j.actaastro.2022.12.039.
21. Koppenwallner, G., Fritsche, B., Lips, T., Klinkrad, H.: SCARAB – A multi-disciplinary code for destruction analysis of Spacecraft during Re-entry. (2005). http://adsabs.harvard.edu/pdf/2005ESASP.563..281K
22. Merrifield, J., Beck, J., Markelov, G., Leyland, P., Molina, R.: Aerothermal Heating Methodology in the Spacecraft Aerothermal Model (SAM). In: Sgobba T., Rongier I. (eds) Space Safety is No Accident. Springer, Cham. (2015). https://doi.org/10.1007/978-3-319-15982-9_53
23. Singh, N., Schwartzentruber, T.E.: Aerothermodynamic correlations for high-speed flow. J. Fluid Mech. (2017). http://dx.doi.org/10.1017/jfm.2017.195
24. Schouler, M., Prévereaud, Y., Mieussens, L. Survey of flight and numerical data of hypersonic rarefied flows encountered in earth orbit and atmospheric reentry. Prog. Aerosp. Sci. (2020). http://dx.doi.org/10.1016/j.paerosci.2020.100638
25. Schouler, M., Prévereaud, Y., Mieussens, L. IXV post-flight reconstruction and analysis of the aerothermodynamic measurements along the rarefied portion of the reentry trajectory. Int. J. Heat Mass Transfer. (2021). http://dx.doi.org/10.1016/j.ijheatmasstransfer.2021.121582
26. Schouler, M., Prévereaud, Y., Mieussens, L. Atmospheric model effect on flight data reconstruction: Application to the early phase of the IXV reentry. Int. J. Comput. Fluid Dyn. (2021). http://dx.doi.org/10.1080/10618562.2021.2016720